



HAL
open science

Design of Low-Altitude Martian Orbits using Frequency Analysis

A. Noullez, K. Tsiganis

► **To cite this version:**

A. Noullez, K. Tsiganis. Design of Low-Altitude Martian Orbits using Frequency Analysis. *Advances in Space Research*, 2021, 67, pp.477-495. 10.1016/j.asr.2020.10.032 . hal-03007909

HAL Id: hal-03007909

<https://hal.science/hal-03007909>

Submitted on 16 Nov 2020

HAL is a multi-disciplinary open access archive for the deposit and dissemination of scientific research documents, whether they are published or not. The documents may come from teaching and research institutions in France or abroad, or from public or private research centers.

L'archive ouverte pluridisciplinaire **HAL**, est destinée au dépôt et à la diffusion de documents scientifiques de niveau recherche, publiés ou non, émanant des établissements d'enseignement et de recherche français ou étrangers, des laboratoires publics ou privés.

Design of Low-Altitude Martian Orbits using Frequency Analysis

A. Noullez^{a,*}, K. Tsiganis^b

^aUniversité Côte d’Azur, Observatoire de la Côte d’Azur, CNRS, Laboratoire Lagrange,
bd. de l’Observatoire, C.S. 34229, 06304 Nice Cedex 4, France

^bSection of Astrophysics Astronomy & Mechanics, Department of Physics, Aristotle University of Thessaloniki,
GR 541 24 Thessaloniki, Greece

Abstract

Nearly-circular *Frozen Orbits* (FOs) around axisymmetric bodies — or, quasi-circular *Periodic Orbits* (POs) around non-axisymmetric bodies — are of primary concern in the design of low-altitude survey missions. Here, we study very low-altitude orbits (down to 50 km) in a high-degree and order model of the Martian gravity field. We apply Prony’s Frequency Analysis (FA) to characterize the time variation of their orbital elements by computing accurate quasi-periodic decompositions of the eccentricity and inclination vectors. An efficient, iterative filtering algorithm, previously applied to lunar orbiters, complements the method and is used to accurately compute the locations of POs/FOs, for a wide range of initial conditions. By defining the ‘distance’ of any orbit from the family of POs and using the relative amplitudes of the different components of the motion, we can build ‘dynamical fate maps’ that graphically depict the survivability of low-eccentricity, low-altitude orbits at every inclination, and can be used for efficient mission planning. While lowering the altitude generally enhances the effect of tesseral and sectorial gravity harmonics, we find this to have less consequence for low altitude Martian satellites, in contrast with the Lunar case. Hence, a high-degree ($\simeq 20^{\text{th}}$) axisymmetric model is adequate for preliminary mission design at moderate altitudes, but should be complemented at low altitudes by the methods described here. All families of POs and their spectral decompositions can be accurately and effectively computed by continuation in arbitrarily complex Martian gravity models, as our filtering algorithm requires only short integration arcs.

Keywords: Satellite Orbits, Mars Orbits, Frozen Orbits, Frequency Analysis

1. Introduction

Efficient design of satellite survey missions is typically based on a set of requirements and operational constraints. For example, the orbital geometry must be suitable for the mission at hand (e.g. low-altitude, near-circular, polar orbit for global surveys), while orbital variations due to the gravitational field of the target body (primary) be such that a reasonable lifetime is ensured, with minimal active control. The complexity of the gravitational field of realistic solar system objects does not necessarily facilitate this task.

Satellite motion around non-spherical bodies has been extensively studied, starting from the axisymmetric ‘ J_2 problem’ (see Allan (1970); Hughes (1981); Coffey et al. (1986); Jupp (1988)), where the only non-Keplerian potential term is the lowest-order zonal one. The general ‘zonal problem’ — in which the disturbing function contains only zonal harmonics of arbitrary order — can be cast into a one degree-of-freedom (d.o.f.) problem, if averaged over the mean motion of the satellite (i.e. ignoring possible tesseral

resonances; see Kaula (1966) and De Saedeleer (2005) for a closed-form theory), such that the mean semimajor axis a of the satellite becomes a constant of motion. The fixed points of this integrable dynamical system are the well-known *Frozen Orbits* (FOs), for which also the inclination i , the argument of pericenter (ω , or g in the usual notation of Delaunay variables) and the eccentricity e all become stationary. The right ascension of the ascending node (nodal longitude, Ω , or h in Delaunay form) precesses at constant rate. Irrespective of altitude, FOs have $g = \pm 90^\circ$ and, for low eccentricities and high inclinations, $e \sim \mathcal{O}(J_3/2J_2 \sin i)$, to a first approximation (Coffey et al., 1994). For an extended discussion on higher degree/order approximations to FOs, the reader is referred to Gurfil and Lara (2013), Lara (2018) or the textbook by Gurfil and Seidelmann (2016). For analytical models of FOs in Lunar orbiter problems, the reader is referred to the works of San-Juan et al. (2008) Abad et al. (2009) and Lara et al. (2009). Knežević and Milani (1998) also developed a canonical analytical theory for the high-order axisymmetric Lunar problem, while Delsate et al. (2010) applied the theory to Mercurian satellites.

If the primary’s potential has a relatively significant deviation from axial symmetry — as is the case for the Moon — it may be necessary to use models of higher

*Corresponding author
Email addresses: anz@oca.eu (A. Noullez), tsiganis@auth.gr (K. Tsiganis)

complexity to adequately describe secular satellite motion. Non-axisymmetric potential terms add a second degree of freedom in the averaged problem and hence FOs with all four elements (a, e, i, g) being constant do not generally exist. Instead, *Periodic Orbits* (POs) of this 2-d.o.f. system can be found, for which i , e and g are not constant but suffer only low-amplitude, fast-periodic variations (see [Tzirti et al. \(2010\)](#)), being however free from “slow”, secular variations. Note that one can also define *Frozen-on-average* orbits in tesseral potentials, removing h -periodic terms through a canonical transformation, as in [Garfinkel \(1965\)](#) for low-Earth orbits. As shown in [Lara et al. \(2013\)](#), inverting the generating function to re-introduce the short-period terms can be used to refine the nominal frozen solution, leading to an h -periodic orbit nearly identical (up to the order of the transformation) to the POs defined above.

Because of the near-preservation of orbital geometry and reduced excursions in orbital elements, periodic orbits are interesting for astrodynamics engineering and have thus received special attention (see e.g. [Lara \(1997\)](#); [Lara \(1999\)](#); [Lara \(2003\)](#); [Tzirti et al. \(2010\)](#) and [Lara \(2011\)](#)). POs would appear as fixed points on a suitably chosen Poincaré section of the 4-d phase space of the averaged problem and they are in general non-isolated, i.e. they form ‘families’ that can be found by locating one such orbit and then smoothly varying some parameter (e.g. the inclination) of the system; this is known as *continuation* method. A well-established method for computing families of period orbits is that of differential corrections ([Deprit and Henrard, 1967](#)). An efficient implementation algorithm can be found in ([Lara and Peláez, 2002](#)). The method also gives information on the linear stability of POs, and can be amended by differential algebra procedures (as in [He et al. \(2017\)](#)) for a more realistic propagation of uncertainties. This method has been successfully applied for finding repeat-groundtrack orbits in high-degree models of the Moon ([Russel and Lara, 2007](#)) and the Earth ([Lara and Russel, 2008](#)).

Recently, in ([Tzirti et al., 2014](#)) and ([Noullez et al., 2015](#)), we studied low-altitude satellite orbits around the Moon, using a novel frequency analysis (FA) algorithm — that we called *Prony’s method* — as a tool for obtaining a global view of the secular dynamics, in arbitrary lunar gravity models. Our numerical FA method is quite efficient, as only short trajectory arcs are necessary for deriving an accurate quasi-periodic decomposition of the orbit; thus it can be applied to large sets of initial conditions. As found by different authors ([Lara et al. \(2009\)](#); [Lara et al. \(2020\)](#)) and confirmed by our own experiments ([Tzirti et al., 2014](#)), a high-degree model is necessary to design low-altitude high-inclination orbits for the Moon, and a ‘minimal’ gravity model should be of degree at least $l \geq 7$ for moderate altitudes and at least $l \geq 9$ for low-altitude polar orbits. Moreover, going to lower and lower altitudes, the POs of non-axisymmetric models become increasingly displaced in (e, g) from the FOs of the corresponding axisymmetric problem, due to the relatively large $C_{2,2}$ and

$C_{3,1}$ terms. The effect of these terms was essentially observed in ([Knežević and Milani, 1998](#)), who found that a satellite starting from a low-altitude FO (found in the axisymmetric model) can crash on the lunar surface, when subjected to a complete lunar gravity model, if no orbit maintenance is performed.

In ([Noullez et al., 2015](#)) we also presented an *iterative filtering algorithm*, as a tool that allows efficient computation of the families of POs of the 2-d.o.f problem. The algorithm is not really ‘new’; it has been ‘rediscovered’ many times in celestial mechanics, for example by [Coutedic et al. \(2010\)](#), who used it to locate stable, resonant periodic orbits in two-planet systems, [Noyelles \(2009\)](#) and [Robutel et al. \(2011\)](#) who studied the 3:2 spin-orbit resonance problem and 1:1 resonant coorbital rotation, [Dufey et al. \(2009\)](#) who analyzed the libration of Mercury, or [Delsate \(2011\)](#) who studied ground-track resonances around Vesta. All these authors used the NAFF method of [Laskar \(1990\)](#), for the frequency analysis part, which requires a trajectory arc that covers at least a few periods of the *slowest*-varying term. In ([Noullez et al., 2015](#)), we used Prony’s FA method that only needs a short trajectory arc to fit all frequencies.

The main idea behind the filtering algorithm is to remove a selected frequency component from the decomposed eccentricity vector — in our case, the slow “proper” mode — to get to a pure *Periodic Orbit* PO that only contains ‘fast’ (forced) terms of low amplitude, overimposed on a quasi-stationary solution. These characteristics of the PO decomposition are explained by the theory of [Wiesel \(2012\)](#), which is devoted to the mathematical construction of near-circular periodic solutions and perturbations thereof, applied to reconstructing the trajectories of particular satellites. Despite the different approach and scope, Wiesel’s elegant work also provides basis for the convergence of our algorithm: it demonstrates the existence of a single, slow ‘proper’ mode for near-periodic solutions and how, by subtracting this component from the solution (see Eq. (39) of that paper) one would be led ideally to a periodic solution (plus higher-order terms), with excursions that do not reduce to zero, in general.

Starting from an educated first guess (e.g. the FO of an axisymmetric model), we first compute the orbital evolution for a short time T ($\simeq 30 \text{ day}_{\otimes}$ in the case of Mars, studied here, \otimes denoting any parameter specific to Mars) to derive the quasi-periodic decomposition of the eccentricity vector. Then, we remove the slow (free precession) component, thus defining a new set of ‘filtered’ initial conditions. Repeating the integration for the new initial condition, we find a new orbit that is actually ‘closer’ to the PO, in the sense that the amplitude of the slow mode is now much smaller than before. As shown in ([Noullez et al., 2015](#)), typically after 2–3 iterations, the method converges to machine precision on the PO, for all initial eccentricities, inclinations and altitudes studied, such that the problem observed by [Knežević and Milani \(1998\)](#) goes away.

In the present paper we apply our FA method to analyze low-altitude orbits in axisymmetric and non-axisymmetric models of the Martian gravity field. Studies of ‘special’ (i.e. *Frozen* or *Sun-synchronous* or *Repeating Ground Track*) orbits around Mars are rather rare (but see the recent papers of Liu et al. (2010), Liu et al. (2011), Liu et al. (2012) or Zhou et al. (2012)), as it is only recently that accurate models of Mars gravity field have been obtained (see Konopliv et al. (2016), Genova et al. (2016) and references therein), so these orbits are still not as well-known as they are for the Earth or Moon and deserve study. We focus on using the iterative algorithm to identify the families of POs and FOs of each model and their differences. We are particularly interested in low-eccentricity POs (or FOs). The importance of such orbits for Mars can be understood by the fact that they are already employed in missions — e.g. the Mars Global Surveyor ($i = 93^\circ$, $e \approx 0.008$, pericenter altitude 372 km). Analytical approaches to the study of their dynamics have been proposed by San-Juan et al. (2011), for an axisymmetric model. Here, we focus on the conditions needed to effectively retain very low altitude, namely a ‘circular altitude’ $a - R_\otimes$ less than 100 km, where a is the semi-major axis of the satellite and R_\otimes the mean equatorial radius of Mars.

In the following sections we first describe some essential characteristics of our models of the Martian gravity field and recall the essentials of Prony’s FA method and the filtering algorithm; the reader is referred to (Tzirti et al., 2014) and (Noullez et al., 2015) for more details. Then, we present our results on the computed families of POs/FOs and the dynamics in their neighborhood. Our conclusions are presented in the last section of this paper.

2. Martian gravity field and dynamical models

Let us examine whether the analytical and numerical tools that we developed for the study of orbits around the Moon (Tzirti et al. (2009); Tzirti et al. (2010); Tzirti et al. (2014); Noullez et al. (2015)) can be readily applied to the case of low-altitude Martian orbits. The two bodies in fact differ significantly, both in terms of their main physical properties, but also in the details of their gravitational field. That being said, the main ingredients needed to apply our formalism are similar, namely (a) wide-enough separation of the three principal frequencies of motion, which allow for smooth (i.e. non-chaotic) dynamics, and (b) availability of a very precise gravity field, which allows for an accurate propagation at low altitudes. For the altitude range considered here, between 0 and 500 km, the Martian gravity field dominates over other effects, like the solar three-body perturbation or the atmospheric pressure, which are neglected here.

2.1. Characteristic time scales

To study the secular motion of a low-altitude (massless) satellite around Mars, we need to average the disturbing function over the mean anomaly l . This is acceptable

	Earth	Moon	Mars
Mass M [kg]	5.972×10^{24}	73.48×10^{21}	641.9×10^{21}
Radius R [km]	6378	1738	3397
Oblateness J_2	1.083×10^{-3}	204×10^{-6}	1.956×10^{-3}
J_3	-2.532×10^{-6}	9.999×10^{-6}	31.94×10^{-6}
T_{rot} [day]	1	27.32	1.026
Satellite at body surface $a = R$			
$e_{\text{F}}(J_2 \& J_3; R, 90^\circ)$	0.0012	-0.0245	-0.0082
$T_{\text{rev}}(R)$ [day]	0.0587	0.0752	0.0696
$T_{\text{s}}(R)$ [day]	18.06	123	11.86
$T_{\text{rot}}/T_{\text{rev}}(R)$	17	363.2	14.75
$T_{\text{s}}(R)/T_{\text{rot}}$	18.06	4.5	11.56
Satellite at 100 km altitude $a = R + 100$ km			
$e_{\text{c}}(a)$	0.0154	0.0544	0.0286
$T_{\text{rev}}(a)$ [day]	0.06	0.0818	0.0727
$T_{\text{s}}(a)$ [day]	19.08	149.5	13.12
$T_{\text{rot}}/T_{\text{rev}}(a)$	16.6	334	14.12
$T_{\text{s}}(a)/T_{\text{rot}}$	19.08	5.7	12.79

Table 1: Main physical parameters for the Earth, Moon and Mars. Averaging over the mean anomaly fast angle l of a satellite is allowed, provided the mean motion $n_{\text{rev}}(a) \equiv 2\pi/T_{\text{rev}}(a) \approx (\mathcal{G}M a^{-3})^{1/2}$ (for non-spherical primaries, this Keplerian approximation to the mean motion should be corrected at least for the oblateness J_2 that slightly accelerates the revolution frequency; see Murray and Dermott (1999) or Gurfil and Seidelmann (2016)) is much larger than the *forced motion* angular frequency $2\pi/T_{\text{rot}}$ due to the primary’s rotation. Also, to avoid resonances, the forced frequency and the slow free precession rate of the pericenter $\dot{\varphi} = 2\pi/T_{\text{s}}(a)$ (computed here for $e = i = 0$ and accounting only for J_2) should be well separated. Both conditions are well satisfied for low-altitude orbits around all three primaries shown here. Eccentricity $e_{\text{F}}(J_2 \& J_3; R, 90^\circ)$ is the maximum eccentricity for the location of *Frozen Orbits* computed in the ‘ $J_2 \& J_3$ problem’ at $i = 90^\circ$ and at the body surface R , while orbits with eccentricity larger than $e_{\text{c}}(a)$ at altitude a will collide with the body surface (note that $e_{\text{c}}(R) = 0$). Also note the different signs of J_3 for the Moon and Mars with respect to the Earth.

when the mean motion, $n_{\text{rev}}(a)$ is fast enough and well-separated from all other frequencies present in the problem: (i) the mean rotation rate $2\pi/T_{\text{rot}}$ of the primary, which introduces a periodic forcing on the satellite orbit, and (ii) the (slow) precession rate of the pericenter argument g . Using the formulae of the averaged ‘ J_2 problem’ (see e.g. Gurfil and Seidelmann (2016)) one gets

$$\dot{g}(a, e, i) = 3 J_2 n_{\text{rev}}(a) \frac{5 \cos(2i) + 3}{8(1 - e^2)^2} \left(\frac{R_{\otimes}}{a} \right)^2 \quad (1)$$

which is as small as $\mathcal{O}(J_2)$. Table 1 lists the three characteristic periods for the Earth, Moon and Mars, and shows that the separation factor between the different frequencies is always in the range $\simeq 12$ –14 for Mars. Note that the wide separation of the frequencies ensures that low-order resonances and chaotic phenomena are not present in the motion, and hence a meaningful quasi-periodic decomposition can be found by Frequency Analysis.

2.2. Martian gravity models and equations of motion

The Martian gravitational potential can be expressed as a spherical harmonics expansion in the body-fixed reference frame (Kaula, 1966)

$$V = -\frac{\mu}{r} \sum_{l=0}^{\infty} \left(\frac{R_{\otimes}}{r} \right)^l \times \sum_{m=0}^l P_{l,m}(\sin \phi) [C_{l,m} \cos m\lambda + S_{l,m} \sin m\lambda], \quad (2)$$

where $\mu = \mathcal{G}M_{\otimes}$ is the mass parameter and R_{\otimes} is the mean equatorial radius of Mars (3397 km), (ϕ, λ) are the planetocentric latitude and east longitude respectively, r the distance of the satellite to the center of Mars, $C_{l,m}$ and $S_{l,m}$ the non-normalized adimensional gravitational coefficients, and $P_{l,m}$ the associated Legendre polynomials of degree l and order m . For $m = 0$ we get the zonal harmonic coefficients, for which we will use the notation $J_l = -C_{l,0}$. To integrate trajectories and use our technique to find low-altitude orbits around a specific object, these coefficients have to be determined beforehand, either from the perturbations of the orbit of a relatively high-flying first satellite, or from a shape model coming from e.g. radar observations. In this work, we have made preliminary trials using different Mars gravity models of high degree and order, that is models MGS95J and MR0120D, coming from JPL (see Konopliv et al. (2006), Konopliv et al. (2011), Konopliv et al. (2016) and references therein for a description), and Goddard Mars models 2B GMM-2B and model 3 GMM-3, described in (Lemoine et al., 2001) and (Genova et al., 2016).

Of course, increasing (l, m) the model becomes more and more accurate, but also less and less tractable, as the number of terms increases quadratically with degree. Thus, as we did also in (Noullez et al., 2015), we tried to define a ‘minimum model’ for the purposes of this study, by progressively increasing the truncation degree l_{max} from 8

to 24 and computing FOs and POs at a few selected inclinations with initial altitude $a_0 = R_{\otimes} + 60$ km. This is a procedure similar to the one used by (Liu et al., 2011) for Mars orbits with a minimum altitude of 200 km. Systematic strategies to assess the minimal truncation order, needed to reach a given accuracy for different altitudes and inclinations were presented in (Lara, 2018) for the Earth, and (Lara et al., 2020) for the Moon, always based on progressively increasing the degree and checking the convergence of orbits to a given accuracy. We found the results to vary substantially up to $l_{\text{max}} \approx 20$ (much higher than $l_{\text{max}} = 9$ used by (Liu et al., 2011), as we are dealing with lower altitudes), beyond which the trajectories have very comparable secular evolutions; also, for $l_{\text{max}} \leq 20$, all JPL and Goddard models gave similar results. Hence, we decided to adopt the Goddard Mars model 2B GMM-2B throughout this paper, truncated at $l_{\text{max}} = 20$ and including all $0 \leq m \leq l$ terms, that we will now refer to as 20DM model. To quantify the effects of non-axisymmetric terms, we also employed a simpler 20ZM model, for which only the zonal terms J_2 – J_{20} are retained to obtain an axisymmetric degree 20 model.

It is customary to employ the *normalized* gravity coefficients $\bar{C}_{l,m}$ and $\bar{S}_{l,m}$, and fully normalized associated Legendre polynomials $\bar{P}_{l,m}$, to quantify the relative importance of terms in the above expansion (Kaula, 1966)

$$\begin{pmatrix} \bar{P}_{l,m} \\ \bar{C}_{l,m} \\ \bar{S}_{l,m} \end{pmatrix} = \left[\frac{(l-m)! (2l+1) (2-\delta_{0,m})}{(l+m)!} \right]^{1/2} \begin{pmatrix} P_{l,m} \\ C_{l,m} \\ S_{l,m} \end{pmatrix}. \quad (3)$$

Figure 1 is a graphic representation of the normalized gravitational coefficients $\bar{J}_{l,m} \equiv (\bar{C}_{l,m}^2 + \bar{S}_{l,m}^2)^{1/2}$ for both Moon and Mars. The relative strength of harmonics decreases rapidly with circular altitude $a - R$ and degree l , as $(R/a)^l$, following ‘Kaula’s rule’, i.e. $\bar{J}_{l,m} \sim l^{-2}$. Such figures can be useful for comparing the relative importance of gravitational coefficients between two bodies, but also for assessing which (if any) can be neglected, to some approximation. For instance, for the Moon, J_5 is much smaller than the ‘mean’ and likely does not contribute as significantly to the dynamics as other coefficients of both higher and lower degree. Also, J_2 does not over-dominate the other terms, as $C_{2,2}$ is nearly as large. Coefficients $C_{3,1}$ and J_7 appear on the other hand abnormally large and, as already noted by several authors (from (Elife and Lara, 2003) to (Tzirti et al., 2014)), they need to be taken into account for low-altitude lunar satellites. Note, however, that the figure should not be taken at face value, as different terms have different effects, depending on the geometry of the orbit considered and, in particular, higher-degree coefficients are more and more important at lower altitudes and larger inclinations. For example, the Moon’s J_9 that falls right on the ‘mean’, controls the location of FOs at low-altitude polar orbits, as noted by (Lara et al., 2009) and (Lara, 2011) (this is also related to the very low values of J_{11} , J_{13} and J_{15} , evident in figure 1).

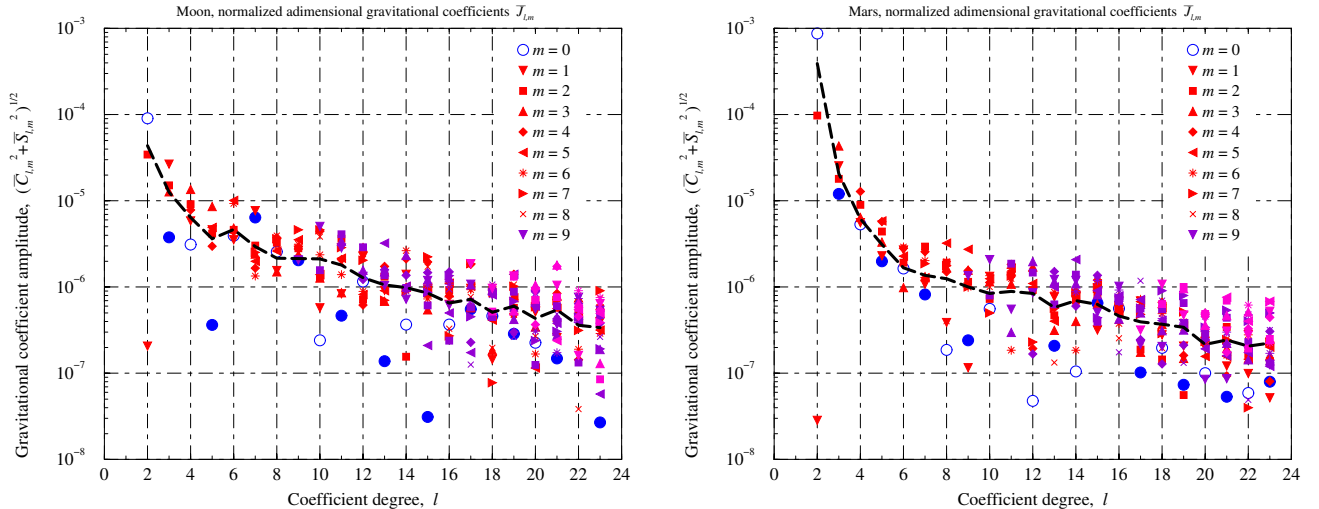


Figure 1: Normalized gravitational coefficients $\bar{J}_{l,m} \equiv (\bar{C}_{l,m}^2 + \bar{S}_{l,m}^2)^{1/2}$ for the Moon (left) and Mars (right) shown at the same scale, as a function of degree l . Different orders m are shown with different symbols and colors (red, violet, magenta). Zonal coefficients $m = 0$ are shown as blue circles, empty \circ for even degree l and filled \bullet for odd degree. The thick dashed line is the degree mean amplitude $[\sum_{m=0}^l \bar{J}_{l,m}^2 / (2l + 1)]^{1/2}$ as a function of degree l , and decays approximately as l^{-2} (Kaula’s rule, see [Kaula \(1966\)](#)).

For Mars, the situation is different, as J_2 dominates the dynamics, although not as much as for Earth. $C_{2,2}$ is relatively large — only 10 times smaller than J_2 — while it is 2 orders of magnitude smaller for Earth. In general, higher-degree terms and $m \neq 0$ terms are relatively stronger for Mars with respect to low- l and $m = 0$ terms, comparing to Earth. Hence, we expect the secular motion of low-altitude satellites around Mars, Earth and the Moon to be quite different.

In the Hamiltonian description, the motion of a satellite in the 20DM model takes the form

$$\mathcal{H}_n = \mathcal{H}_0 + \sum_{l=2}^{l_{\max}} \mathcal{H}_{l,0} + \sum_{l=2}^{l_{\max}} \sum_{m=1}^{l-1} \mathcal{H}_{l,m} + \sum_{l=2}^{l_{\max}} \mathcal{H}_{l,l} + \mathcal{H}_{n_{\otimes}}, \quad (4)$$

where $\mathcal{H}_0 = |\mathbf{u}|^2/2 - \mu/r$ is the Keplerian part (\mathbf{u} is the satellite’s velocity), $\mathcal{H}_{l,0}$, $\mathcal{H}_{l,m}$, $\mathcal{H}_{l,l}$ describe respectively the zonal, tesseral and sectorial gravity harmonics and $\mathcal{H}_{n_{\otimes}} = -n_{\text{rot}} H$ is added when working in a Mars-fixed rotating frame. The Hamiltonian is then expressed in canonical Delaunay variables (l, g, h, L, G, H) , where $L = \sqrt{\mu a}$, $G = L \sqrt{(1 - e^2)}$ and $H = G \cos i$, and it is averaged over the mean anomaly l of the satellite in closed form. This procedure — which is valid for arbitrarily high eccentricity — is described in ([De Saedeleer, 2005](#)) and ([Tzirti et al., 2010](#)). Other approaches for constructing the averaged Hamiltonian can be used and, in a recent work by [Lara et al. \(2020\)](#), the use of Kaulas’ recursions ([Kaula, 1966](#)) is pointed out as the most efficient method. Our symbolic code for this procedure is written in `Mathematica` and was checked against ([De Saedeleer, 2006](#)), ([Kaula, 1966](#)) and ([Knežević and Milani, 1998](#)). The symbolic code produces `FORTRAN` expressions that are inserted into a propagation code, which gives the time evolution of (e, i, g, h) ; we re-

mind that the semi-major axis a is constant in the averaged problem.

3. Frequency Analysis applied to Martian orbiters

Frequency Analysis is a powerful tool of time series analysis, and is particularly useful for planetary or satellite orbits, as it provides a quasi-periodic decomposition of the eccentricity and inclination vectors. A (real or complex) quasi-periodic “signal” $u(t)$, is decomposed into a set of p periodic components

$$u(t) = \sum_{k=1}^p \alpha_k e^{i2\pi\nu_k t}, \quad (5)$$

with (real) frequencies ν_k and (complex) amplitudes α_k , using a sample of the signal over an “arc” of duration T , i.e. a finite number N of discrete values of $u[n]$, separated by a constant time interval Δt

$$u[n] \equiv u(n \Delta t) \quad n = 0, \dots, N - 1 \quad (6)$$

$$= \sum_{k=1}^p \alpha_k \rho_k^n \quad \rho_k \equiv e^{i2\pi\nu_k \Delta t}. \quad (7)$$

Different ways of computing the spectrum of $u[n]$ exist, as we described in detail in ([Tzirti et al., 2014](#)). The most common method is that of computing numerically the Fourier transform of $u[n]$, assuming all frequencies ν_k to be of the form $\nu_k = k/T$. The most refined version of this method is Laskar’s NAFF algorithm ([Laskar, 1990](#)) (see also [Laskar \(2005\)](#) or [Laskar et al. \(1992\)](#)). The main shortcoming of Fourier-based methods is that they are based on *averaging* the signal, thus requiring T to be (much) larger than the slowest mode that we need to resolve.

3.1. Prony's Frequency Analysis method

In (Tzirti et al., 2014) we presented ‘Prony’s method’, which is a *fitting* method; this takes away the large- T limitation, so that short signal arcs are capable of capturing long-term oscillations. We repeat here only the essentials of the method and refer the reader to (Tzirti et al., 2014) or (Noullez et al., 2015) for more details.

Prony’s FA method is in fact the complex version of Prony’s original method for real exponentials (de Prony, 1795) (see a modern description in (Hamming, 1973), (Hildebrand, 1987), (Kay, 1988) or (Noullez, 2009)), used to describe the time evolution of pressure in gas expansion. The main ingredient of the method is that any discretely sampled signal that is a simple sum of p exponentials as in (7) obeys a *linear* constant coefficients difference equation of order p

$$u[n] + a_1 u[n-1] + \dots + a_p u[n-p] = 0, \quad (8)$$

and the p complex ‘resonances’ ρ_k are the roots of the characteristic polynomial

$$\rho^p + a_1 \rho^{p-1} + \dots + a_{p-1} \rho + a_p = 0 \quad (9)$$

of this difference equation.

Prony realized that this gives a method to determine the frequencies, because finding the so-called *prediction coefficients* a_j is a *linear* problem that we can solve exactly as soon as we have at least $N \geq 2p$ signal values. To do that, we write equation (8) for $n = p, \dots, 2p-1$ and solve the resulting $p \times p$ linear system

$$\sum_{j=1}^p u[n-j] a_j = -u[n] \quad n = p, \dots, 2p-1 \quad (10)$$

for the p unknown a_j , $j = 1, \dots, p$. Once the prediction coefficients are determined, ρ_k , $k = 1, \dots, p$ are found as the (complex) roots of the polynomial (9), using any standard algorithm (e.g. Newton’s method in the complex plane), with a precision only limited by numerical accuracy (see Hamming (1973) or Hildebrand (1987)), and the frequencies ν_k are then simply obtained as

$$\nu_k = \text{Im} \{ \log(\rho_k) \} / 2\pi \Delta t = \text{Arg}(\rho_k) / 2\pi \Delta t \quad (11)$$

because of the definition of ρ_k eq. (7).

Once the frequencies ν_k are known, the amplitudes α_k , $k = 1, \dots, p$ can be found easily, as the problem is linear in α_k and we only need to solve another $p \times p$ linear system

$$\sum_{k=1}^p \rho_k^n \alpha_k = u[n] \quad n = 0, \dots, p-1. \quad (12)$$

Even if the method is in theory *exact* — save for solving the polynomial (9) — the presence of noise would force us to use a *least-squares* Prony’s method (see e.g. Kay (1988)), and so N should be (much) larger than $2p$, to allow accurate determination of p frequencies. Hence, the

two *linear* problems described above become *optimization* problems that should be solved for increasing values of p , until the decomposition matches the signal to a pre-defined accuracy. Note that Prony’s method assumes only distinct roots ρ_k but, as we move in parameters space, distinct frequencies may collapse, or a frequency may become null (e.g. \dot{g} at the critical inclination). Prony’s method can be adapted to include secular drift terms and circumvent these issues, as described in (Tzirti et al., 2014).

3.2. Spectral decomposition of orbits

We apply Prony’s FA on the two complex variables

$$u(t) \equiv e(t) \times e^{ig(t)} \quad (13)$$

$$v(t) \equiv \sin(i(t)) \times e^{ih(t)}, \quad (14)$$

i.e. the complex representations of the eccentricity and inclination vectors that determine secular motion. From the point of view of signal analysis, they have the advantage of being continuous when the g and h angles go through 2π ; also, the frequencies measured by FA are exactly related to \dot{g} and \dot{h} , and their sign (prograde or retrograde) can be also determined, while analyzing $e(t)$ or $i(t)$ would prevent access to that information, as the spectrum of real variables is always symmetric (hermitian) between ν and $-\nu$.

Orbital propagation is performed with an Adams predictor-corrector scheme, and the vectors are sampled at equidistant intervals Δt ; the sampling time has to satisfy the Nyquist criterion and thus must be chosen smaller than (half) the highest frequency. In the averaged problem, this is the rotational (forcing) frequency of Mars (i.e. the inverse of 1 Martian day), multiplied by l_{max} . We employ a sampling time $\Delta t = 0.02 \text{ day}_{\otimes}$ or $1/50$ of a Martian day¹.

The total length of the signal should be $N \gg 2p$, and also such that the slowest mode must have had the time to vary ‘significantly’. In practice, as we found in (Tzirti et al., 2014), we need N to be at least about $1/8^{\text{th}}$ of the slowest period. We decided to employ $T = 30 \text{ day}_{\otimes}$ (i.e. $N = 1500$ points), which allows reaching machine precision for all frequencies and amplitudes, down to $\nu \approx 0.004 \text{ day}_{\otimes}^{-1}$ for nearly all initial values of (i_0, e_0) at given initial circular altitude $a_0 - R_{\otimes}$. Still, our trajectory arc and data length N is at least an order of magnitude shorter than what traditional Fourier-based methods would need, for the same accuracy.

4. Global view of low-altitude dynamics

We wish to obtain a global view of the dynamics, building a frequencies and amplitudes ‘map’, for a wide range of initial conditions, at sufficient resolution. We restrict

¹From now on, we will express times in units of Martian sidereal $\text{day}_{\otimes} \equiv T_{\text{rot}} = 1.025957$ Earth days, and frequencies in units of $\text{day}_{\otimes}^{-1}$.

ourselves to low altitudes, down to a few tens of kilometers. Performing test integrations, we found that the altitude range 50–500 km has similar dynamics, apart from the percentage of colliding orbits at low altitudes $a_0 - R_\otimes$. Hence, we present here the complete results only for $a_0 = R_\otimes + 60$ km. All orbits have $h_0 = 0$; this only controls the initial phase of the fast periodic component on the orbit. In a similar way, g_0 controls the initial phase of u . As we want this to be close to a FO/PO, we set it equal to $g_0 = -90^\circ$. As shown in (Delsate et al., 2010), the position of FOs is controlled by the odd-order zonal harmonics, and J_3 for Mars has the same sign (positive) as for the Moon, opposite to Earth.

Our FA maps are obtained for orbits starting on a $i_0 - e_0$ grid, spanning the range $0 < i_0 \leq 90^\circ$ and $0 < e_0 < e_c$, where

$$e_c \equiv \frac{a_0 - R_\otimes}{a_0} \quad (15)$$

is the collision eccentricity for circular altitude $a_0 - R_\otimes$, for which the satellite will crash on Mars surface.

The quasi-periodic decompositions of $u(t)$ and $v(t)$ take the form (in order of increasing frequencies)

$$u(t) = \alpha_0 + \alpha_s e^{i2\pi\nu_s t} + \sum_{k \neq 0} \alpha_k e^{i2\pi k\nu_1 t} \quad (16)$$

$$v(t) = \sum_{k \neq 0} \beta_k e^{i2\pi k\nu_1 t} \approx \sin(i_0) e^{i2\pi\nu_1 t} \quad (17)$$

with basic frequencies $\nu_0 \equiv 0$ (constant), ν_s and ν_1 . An example of the decomposition of the eccentricity vector $u(t)$ is given in figure 2, with the first constant term α_0 shown as the thick black star; the second term of (16) is displayed as the dotted blue curve, describing a circle of radius α_s in the complex plane, traveled along at constant angular velocity $2\pi\nu_s$. The sum in the third term of (16) is represented by the thick red curve that closes itself after a period $1/\nu_1$. The full eccentricity vector $u(t)$ is the sum of all three terms and is shown as the thin black line, with full black circles separated in time by one Martian day. The two frequencies ν_s and ν_1 are in general incommensurate, so the curve for $u(t)$ doesn't close itself.

Terms related to the 'fast' frequency ν_1 are present in both $u(t)$ and $v(t)$. These are *forced terms*, related to the rotation of Mars and the (slow) regression of h (caused mainly by the J_2 term at small inclinations), whose rate in the ' J_2 problem' is

$$\nu_1 = \frac{1}{2\pi} \left(\dot{h}(a, e, i) - n_{\text{rot}} \right) \quad (18)$$

$$\dot{h}(a, e, i) \approx \frac{-3}{2} J_2 n_{\text{rev}}(a) \frac{\cos(i)}{(1-e^2)^2} \left(\frac{R_\otimes}{a} \right)^2 \quad (19)$$

Note that $\nu_1 \approx -1 \text{ day}_\otimes^{-1}$, accelerates only by $\approx 4\%$ as i_0 goes from $i_0 = 90^\circ$ to $i_0 = 0$ (see figure 3) and depends only mildly on e_0 . Hence, it is practically a function of i_0 only, for low-altitude Martian orbits. For $v(t)$, only the single frequency ν_1 is present, the amplitude stays nearly

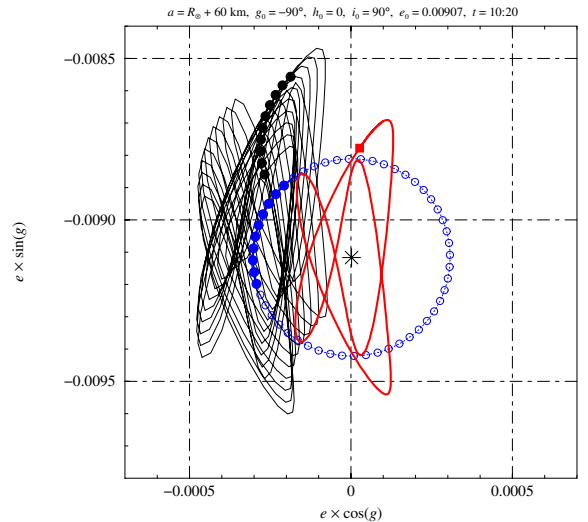


Figure 2: Graphic representation of the frequency decomposition of the eccentricity vector $u = e \cos(g) + i e \sin(g)$ for a Martian polar orbit with $i_0 = 90^\circ$, $e_0 = 0.009$, $g_0 = -90^\circ$ and $h_0 = 0$, at $a_0 = R_\otimes + 60$ km. The thin black line is the 30-days integration, and the full black circles, attached to this line, are separated by a time interval of 1 day_\otimes , showing stroboscopically the slow eccentricity drift. The black star denotes the constant found in the spectral decomposition, corresponding to the *Frozen Orbit* $\alpha_0 \equiv i e_F \sin g_F$, the dotted blue circles corresponds to the (extrapolated with empty circles) proper motion of g (the single 'slow' circular term of frequency ν_s), while the thick red line shows the sum of all the *forced* terms of the decomposition of frequencies $k\nu_1$. The sum of these three components gives a very accurate reconstruction of the black line.

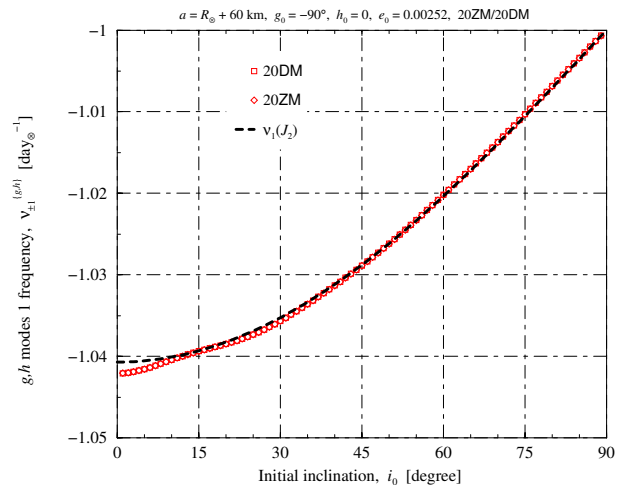


Figure 3: *Forced motion* frequency ν_1 of the g and h angles for the 20DM (squares) and 20ZM model (diamonds) for $g_0 = -90^\circ$, $h_0 = 0$, $e_0 = 0.00252$ and an altitude 60 km, as a function of the inclination i_0 . The periodic frequency of both angles is the same and is independent of g_0 and h_0 , and it is exactly equal to $-n_{\text{rot}}/2\pi \equiv -1.0 \text{ day}_\otimes^{-1}$ for $i_0 = 90^\circ$. The dashed curve is the frequency $-n_{\text{rot}}/2\pi$ corrected by the effect of the J_2 coefficient (eq. (19)), that gives the main contribution to the slight retrograde motion of the node longitude h . Note also that for Mars, the tesseral and sectoral coefficients have no apparent effect on the frequency ν_1 .

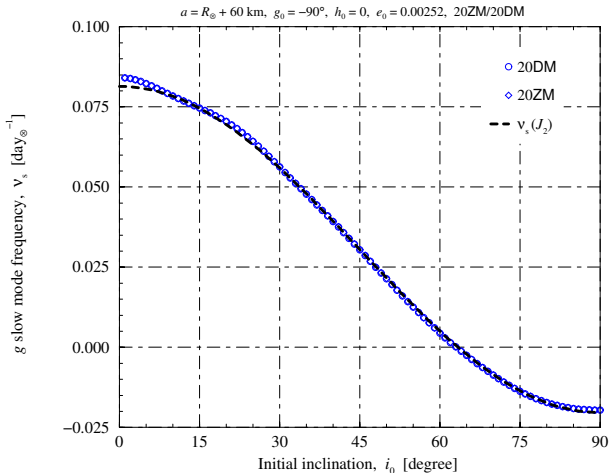


Figure 4: *Proper motion* frequency ν_s for the g angle for the 20DM (circles) and 20ZM model (diamonds) for $g_0 = -90^\circ$, $h_0 = 0$, $e_0 = 0.00252$ and an altitude 60 km, as a function of the inclination i_0 . This slow frequency is almost independent of g_0 and h_0 , has a period that is at least 12 day_\otimes ($\nu_s < 0.085 \text{ day}_\otimes^{-1}$) at that altitude, and goes to zero around $i_0 \sim i_c \approx 63^\circ$. The dashed line is the frequency that would be due to the effect of the J_2 coefficient *only* at that altitude (eq. (1)), and one can see that it gives the main contribution to the proper frequency ν_s . Once again, the axisymmetric and full model frequencies are undistinguishable.

constant at its initial value $\sin(i_0)$ and h circulates freely at constant rate. The fast dynamics of (h, i) is thus essentially unaffected by the motion of the pericenter (g, e) , but it mildly affects the latter through the non-axisymmetric terms of the gravity field of the rotating primary.

The most significant eccentricity variations are due to the second term in (16) that corresponds to the slow *proper* frequency ν_s that, as we can see in figure 4 is indeed well separated from $n_{\text{rot}}/2\pi \simeq 15$ and from $\nu_1 \simeq 1$, taking values in the range $[-0.020, 0.085] \text{ day}_\otimes^{-1}$ as a function of i_0 , and is very close to $\dot{g}/2\pi$ as computed by Eq.(1). The slight deviations seen at small inclinations are primarily caused by the $C_{2,2}$ term. Again, ν_s depends only mildly on e_0 . However, the corresponding amplitude α_s depends strongly on both i_0 and e_0 , as shown in figure 5.

The constant term α_0 of frequency $\nu_0 \equiv 0$ corresponds to the mean position of $u(t)$, around which the orbit is librating. Its value is, in general, *not* equal to the mean of the signal \bar{u} over T , since the other terms would average to zero only if T is an integer multiple of both $1/\nu_s \equiv T_s$ and $1/\nu_1 \approx T_{\text{rot}}$. We also stress that it is only thanks to the fitting properties of Prony’s FA that this term can be determined accurately, using only a short orbit arc. For all orbits where this term is non-negligible, the amplitude α_0 is found purely imaginary, with complex phase $\text{Arg}(\alpha_0) = \pm 90^\circ$. Hence, if we write $\alpha_0 \equiv i e_F \sin g_F$, the *mean* position of the pericenter is $g_F = \pm 90^\circ$, as for *Frozen Orbits* in the axisymmetric problem. In fact, (e_F, g_F) are almost exactly those of the FOs of 20ZM, as we verified – both models give the same α_0 and the orbits *freeze* in eccentricity e and pericenter g , when integrated in 20ZM. Of course,

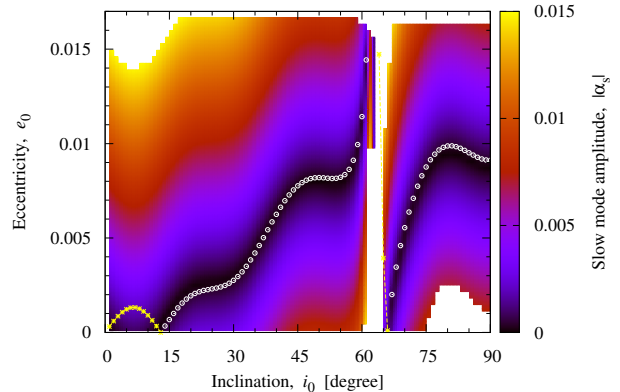


Figure 5: Slow mode amplitude $|\alpha_s|$ as a 2-d grey levels map in the plane of initial conditions $i_0 - e_0$, with fixed initial orientation angles $g_0 = -90^\circ$ and $h_0 = 0$. White zones indicate orbits colliding in less than 30 days. Superposed on top are the location of *Frozen Orbits* FOs eccentricity $e_F \equiv |\alpha_0|$ found by FA for which the pericenter argument g_F is -90° (white circles) or $+90^\circ$ (yellow stars). The regions with minimum slow mode amplitude $|\alpha_s|$ closely follows the FO with the same orientation, and the slow mode amplitude increases linearly when moving away from the FO with the same direction, and even quicker when it has the opposite direction. This leads to collisions with the Martian surface at high eccentricity for $i_0 < 13^\circ$, all eccentricities around the critical angle $i_0 \sim 63^\circ$, and at *low* eccentricities for $i_0 > 75^\circ$.

these initial conditions do *not* ‘freeze’ exactly in 20DM (as we will see in section 5). Again, α_0 has strong variations with i_0 (circles and stars in figure 5, and squares in the left of figure 6), but is found to depend only mildly on e_0 (right of figure 6).

In figure 5, one can see that, when g_F and g_0 have the same sign, the amplitude $|\alpha_s|$ isolines closely follow the variations in position of the FO $e_F \sin g_F$, which denotes both the mean position of the 2-d.o.f. PO *and* the mean position of the full orbit, as both slow and fast modes are periodic with zero mean. The slow motion amplitude is found to increase linearly like $\delta e_F \equiv |e_0 - e_F|$ at any given inclination i_0 . In fact, the proper amplitude $|\alpha_s|$ can be considered as the ‘distance’ of an orbit from the PO at the same inclination. Indeed, for vanishing $|\alpha_s|$, the motion becomes strictly periodic at frequency ν_1 for POs (‘frozen’ for FOs in 20ZM). The fact that $|\alpha_s| \sim \delta e_F$ is probably a consequence of the large separation between the frequencies ν_s and ν_1 that leads to nearly decoupled evolution, as noted in the previous section. Still, $u(t)$ has a non-zero periodic component that slightly separates the true POs from the FOs (see figure 7), and complicates the search for initial conditions for POs (section 5).

Figure 6 shows a graph of $e_F \equiv |\alpha_0|$, $|\alpha_s|$ and α_p for given initial eccentricity e_0 (shown as the thin horizontal line on the left) as a function of initial inclination i_0 (left), and for given initial inclination $i_0 = 90^\circ$, as a function of initial eccentricity e_0 vertically (right), both with $g_0 = -90^\circ$. The amplitudes $|\alpha_k|$ of all modes $\pm k \nu_1$ for $u(t)$ are found to vary only slightly with e_0 (see right of figure 6), depending mostly on i_0 , but the total forced amplitude α_p

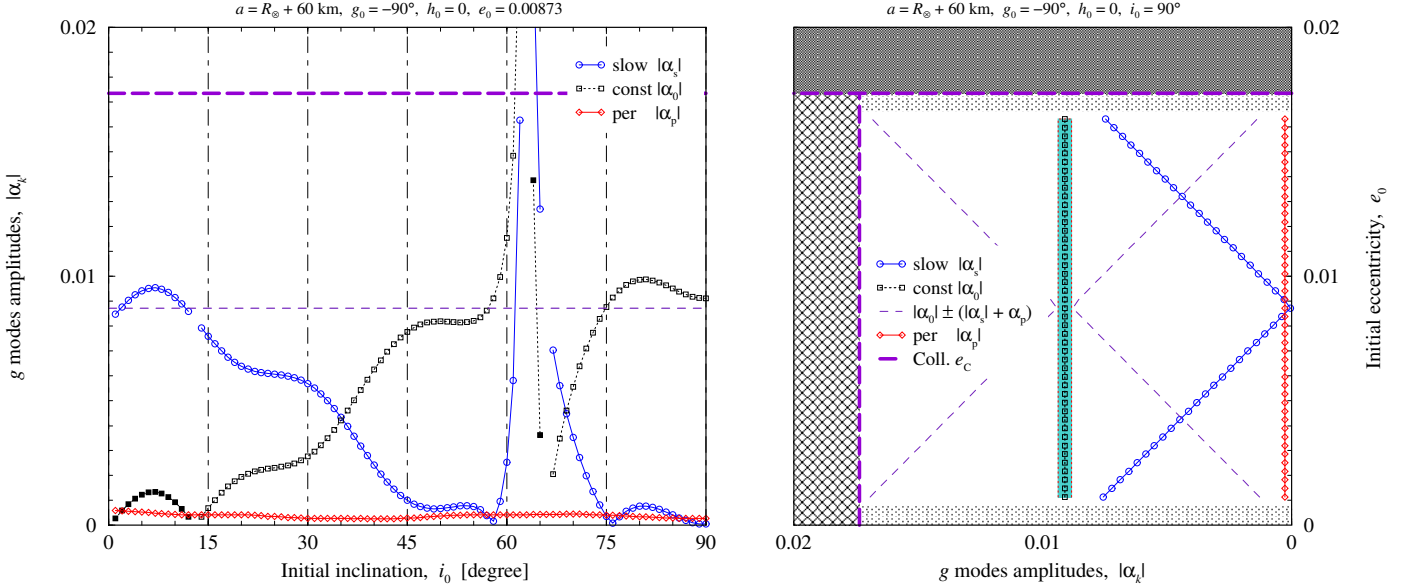


Figure 6: One-dimensional cuts in the map of initial conditions for the FA amplitudes, on the left along i_0 (horizontally) for a constant initial $e_0 = 0.00873$ (shown as dashed thin horizontal line on the left), and on the right along e_0 (vertically) for $i_0 = 90^\circ$, both for fixed initial orientation angles $g_0 = -90^\circ$ and $h_0 = 0$. The three curves in the two graphs are the slow mode amplitude $|\alpha_s|$ (blue circles), the constant amplitude $e_F = |\alpha_0|$ (black squares, empty if $g_F = -90^\circ$, filled if $g_F = +90^\circ$) and the total periodic amplitude α_P (red diamonds). Around $i_0 \sim 63^\circ$, orbits collide with Mars in less than 30 day_\oplus and cannot be analyzed. The dashed thick violet lines on the left and right correspond to the collision eccentricity $e_c = 0.0174$ at that altitude. Orbits will collide with Mars surface (crossed or hatched zones on the right) if $|\alpha_0| \pm \alpha_P$ (grey zone on the right), added to $\pm |\alpha_s|$ (thin blue lines on the right) reaches the collision eccentricity e_c , which can occur at either high or low initial eccentricity e_0 .

defined as $\alpha_p^2 \equiv \sum_{k \neq 0} |\alpha_k|^2$ does not vary much with i_0 . Though α_p is generally small compared to the other two terms, it never goes to zero, so that FOs with *constant* orbital elements do not exist in a non-axisymmetric gravity model and POs are frozen in the strict sense *only* when averaged over the period $1/\nu_1$ (see also Lara et al. (2013)). Note that ν_1 and ν_s are both practically identical between the full (20DM) and the corresponding 20ZM axisymmetric model.

In many applications, the amplitudes $|\alpha_0|$, $|\alpha_s|$ and α_p are *more* interesting than the frequencies: they correspond to the mean eccentricity (for $|\alpha_0|$), the proper eccentricity² $|\alpha_s|$ and a ‘fast’ periodic kick α_p . Depending on the relative sizes of these amplitudes, the orbit will be circulating in g if $|\alpha_0| < |\alpha_s| + \alpha_p$, or librating otherwise. If g_0 has the same sign as g_F , $|\alpha_s| + |\alpha_0| \approx e_0$, so that $|\alpha_s| \approx \delta e_F$. This implies that the amplitude $|\alpha_s|$ decreases when going towards and vanishes at the PO, ‘pointing’ to its location (see figure 6 (right)). Thus, Prony’s FA method provides a measure of orbital ‘distance’ from the relevant PO.

The magnitude $|u(t)|$ is equal to the instantaneous eccentricity $e(t)$. If $e(t_c) \approx e_c$ for some time t_c , the satellite crashes on the Martian surface; this occurs when the sum in (16) equals e_c but, because the frequencies ν_s and ν_1 are well separated and non-commensurate, it suffices that $e_{\max} \equiv |\alpha_0| + |\alpha_s| + \alpha_p \approx e_c$ for the satellite to crash in a time at most $T_s/2 + T_{\text{rot}}$ (half a secular cycle).

Given the above discussion, it is clear that the orbit can crash *either* if e_F or δe_F are large, which can be both true for $e_0 \approx 0$. This is shown graphically for polar orbits with $a_0 = R_\oplus + 60 \text{ km}$ in the right of figure 6. The orbits crash both for $e_0 > 0.0163$ (less than the collision eccentricity $e_c = 0.0174$) or $e_0 < 0.0011$ (see also figure 5 on how low- e orbits crash for $75^\circ < i_0 \leq 90^\circ$). This is what Knežević and Milani (1998) had noticed for low lunar orbiters and is the reason why a high-degree gravity model and knowing the location of the FOs are necessary for these studies.

5. Locating FOs/POs by filtering

As noted in the previous section, the periodic amplitude α_p never vanishes for a non-axisymmetric gravity model, so *Frozen Orbits* with strictly fixed elements, free from periodic oscillations at frequency ν_1 , do not exist. However, *Periodic Orbits* have proper amplitude $|\alpha_s| = 0$ and will only have very small eccentricity variations (i.e. of size $\sim \alpha_p \simeq 10^{-3}$) and so will have minimum eccentricity and altitude variations for a given i_0 . If we are moreover interested in minimizing altitude variations whatever i_0 , we can search for POs with $e_F \approx 0$. Such POs would have only fast periodic oscillations (amplitudes α_k) around a zero mean eccentricity; the pericenter argument will certainly circulate, but the orbit will be quasi-circular.

In this section, we apply the iterative filtering algorithm presented in (Noullez et al., 2015) to compute the

²As it is usually called in celestial mechanics.

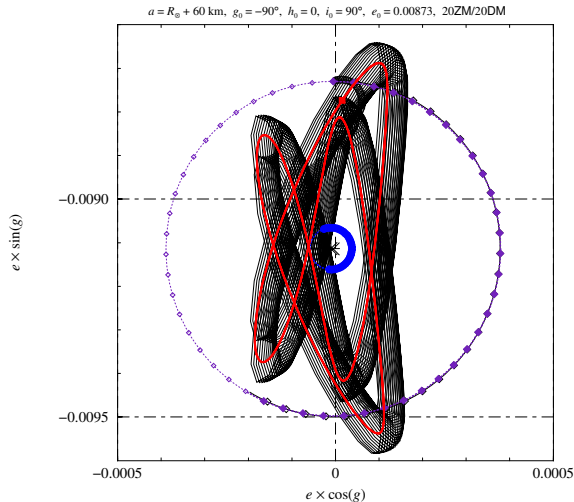


Figure 7: FA decomposition of orbits (thin black lines) started exactly at the same initial conditions for the axisymmetric 20ZM (diamonds) and the full 20DM model (circles). Both orbits share *exactly* the same FO location (shown as a black star), but the axisymmetric orbit only contains a slow proper motion (indigo diamonds) that precisely describes the orbit itself. The full-model orbit also contains a periodic component (red curve obtained by FA) whose instantaneous value has to be subtracted from the initial conditions, to derive the proper motion (blue circles). The PO is found almost exactly if we remove the slow component from the initial orbit, to derive a periodic part that nearly coincides with the PO and whose initial condition is the red square).

locations and spectral decompositions of POs for all values i_0 at given $a_0 - R_\otimes$. We recall that locating a PO for a given i_0 implies finding (e_0, g_0) points in a suitable h_0 section (we took $h_0 = 0$) where the real and imaginary parts of α_s vanish simultaneously. As the complex amplitudes are smooth functions of the initial conditions and we have two ‘free’ parameters (e_0 and g_0) available to cancel the two components of the amplitude α_s , one can expect to find a single periodic solution, for each i_0 and $a_0 - R_\otimes$. Note that ν_s stays constant as α_s goes to 0 when changing e_0 and g_0 , unlike in the ‘ J_2 problem’ where the orbit freezes not because the proper amplitude goes to zero, but because the frequency ν_s vanishes at the critical inclination i_c , so that FOs exist for every e_0 at that particular inclination i_c — however, g must be an integer multiple of 90° , as becomes evident when considering the problem at order $\mathcal{O}(J_2^2)$ or higher; see e.g. (Coffey et al., 1986), (Broucke, 1994), (Gurfil and Lara, 2013) and (Gurfil and Seidemann, 2016).

5.1. Iterative filtering algorithm

One might naively think that the mean orbit position $\alpha_0 \equiv i e_F \sin g_F$ found by Prony’s FA gives the initial conditions (e_F, g_F) of the PO but this is not the case, as figure 7 demonstrates. In fact, α_0 is the position of the FO that can indeed be computed immediately by Prony’s FA, in axisymmetric models. In 2-d.o.f. models, it is necessary to separate the slow and periodic components. Thus, the PO is found only after ‘filtering’ (i.e. removing) the

slow component. But the periodic part has non-zero amplitude on the PO, and is actually needed for computing the PO’s initial condition. This is the basis of the ‘iterative filtering algorithm’ that we will now describe briefly (see Noullez et al. (2015) for details).

As described also in the Introduction, we start the procedure by adopting a first guess $\{u^{(0)}(0), v^{(0)}(0)\} = \{e_0 \exp(i g_0), \sin(i_0) \exp(i h_0)\}$, for which we compute its time evolution for a short integration time T (30 day $_\otimes$) and derive its quasi-periodic decompositions (16) and (17), using Prony’s FA method. Then, we remove the slow component α_s from the reconstructed time series, thus obtaining a ‘filtered’ orbit

$$\begin{aligned} \{\tilde{u}(t), \tilde{v}(t)\} &\equiv \{u(t) - \alpha_s e^{i 2\pi \nu_s t}, v(t)\} \\ &= \left\{ \sum_k \alpha_k e^{i 2\pi k \nu_1 t}, \sum_{k \neq 0} \beta_k e^{i 2\pi k \nu_1 t} \right\}, \end{aligned} \quad (20)$$

which is by construction periodic with frequency ν_1 . This operation does not change $v(t)$, i.e. $\tilde{v}(t) = v(t)$. Hence, the ‘new orbit’ has the same (i_0, h_0) as the original.

If the α_0 and α_k ’s were completely independent of (g, e) , the filtered orbit $\{\tilde{u}(t), \tilde{v}(t)\}$ would be precisely the PO. This is however not true, as the filtered orbit is generally not an exact solution of the equations of motion, for these initial conditions $\{\tilde{u}(0), \tilde{v}(0)\}$. But, given that the main frequencies ν_s and ν_1 are well-separated and no linear combinations with significant amplitude appear in $u(t)$ and $v(t)$, the proper mode defines a circle on the $(e \cos g, e \sin g)$ plane, centered around α_0 . Elimination of the slow term sets the ‘new’ orbit at the center of this circle, adding the small periodic component. Thus, the ‘new’ orbit will have a slow part that is smaller than the original one and closer to the PO.

Using the new initial conditions, we iterate the procedure of integrating and filtering. Here, as in (Noullez et al., 2015) for the Moon, the procedure always converged to a PO in a matter of $r = 2 - 3$ iterations, with a near-exponential decrease of $|\alpha_s|$. However, there is no rigorous proof that this algorithm always converges, despite attempts e.g. by Noyelles et al. (2012). Nevertheless, we did not encounter any case where the algorithm failed. Note also that the computational time for applying Prony’s FA and filtering is negligible with respect to the integration time of the orbit.

5.2. Low-altitude Martian POs

Using our *iterative filtering algorithm*, we computed the POs (g_P, e_P) for an initial altitude $a_0 = R_\otimes + 60$ km, and for $0 < i_0 \leq 120^\circ$. As starting guess we used the FO (e_F, g_F) found by Prony’s FA. The algorithm converged after at most 2–3 iterations, with a residual amplitude $|\alpha_s| \leq 10^{-8}$. The only exceptions to this fast convergence were found near the critical inclination $i_c \approx 63.4^\circ$, where the POs computed eccentricity becomes larger than e_c so that all these orbits would crash on Mars surface. As in (Lara

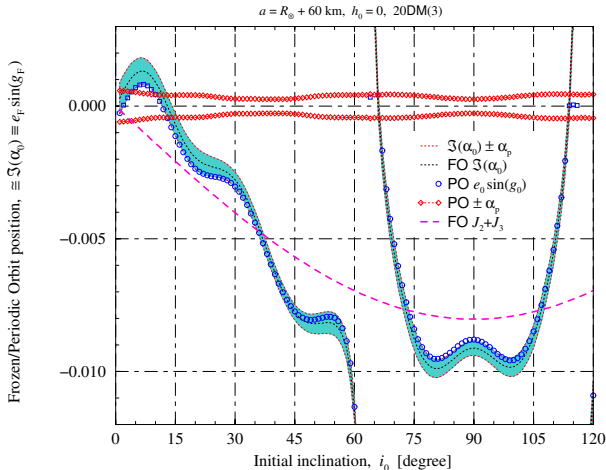


Figure 8: Initial (signed) eccentricity $e_p \sin g_p$ of the POs found after 3 iterations of the filtering algorithm (blue circles), for $0 < i_0 \leq 120^\circ$ (note the symmetry around polar orbits) and $a_0 = R_\oplus + 60$ km. The modulus of the constant term $\pm|\alpha_0|$ that gives the mean position $e_F \sin g_F$ (i.e. FOs of 20ZM) is also shown as a black dashed line. The turquoise band shows the amplitude $\pm\alpha_p$ of the fast, forced motion (also shown as red diamonds around the $e = 0$ axis). The true POs are always close to the FOs (inside the periodic band), but their initial conditions differ due to the periodic part. The dashed magenta line is the locus of FOs in the simple ‘ J_2 & J_3 problem’, which apparently cannot serve better than a good starting point for the algorithm, as it can be far from the true POs (see also figures 9 and 10).

et al., 2009), we display the families of POs using $e_F \sin g_F$ instead of e_F , to avoid an apparent slope discontinuity when g_F jumps between $\pm 90^\circ$ and $\mp 90^\circ$ as e_F goes through zero. For POs, the initial pericenter argument g_p is not exactly $\pm 90^\circ$ and depends slightly on the initial nodal longitude h_0 . However, the amplitude of the periodic motion is small, so that g_p will stay close to $\pm 90^\circ$ in most cases.

Figure 8 shows that indeed $e_p \sin g_p$ and $e_F \sin g_F$ are smooth functions of i_0 and POs are always close to the corresponding FOs, but are not the same. In fact, the PO has variations of width $\pm\alpha_p$ around the FO. The graph also shows that the eccentricity of low-altitude Martian POs will always be small. The discontinuities seen around the critical inclinations $i_c \approx 63^\circ$ or 117° are real, and correspond to inclinations where the PO’s eccentricity grows dramatically and goes above e_c , so that non-collisional orbits cease to exist in these regions. POs with very small mean eccentricity exist for $i_0 \approx 13^\circ$ and $i_0 \approx 66^\circ$ or 114° at 60 km altitude. As we will see in section 6.2, these inclinations allow to reach even lower altitudes. The PO’s pericenter argument is always close to $\pm 90^\circ$, except for very low inclinations, where g_0 is determined only by the periodic component and is ill-defined, as $e \rightarrow 0$. POs generally have $g = -90^\circ$, except for $0 < i_0 < 13^\circ$ and around $i_0 = 66^\circ$ or $i_0 = 114^\circ$; these are the only inclinations at this altitude for which we can get stable POs with g in the Northern hemisphere.

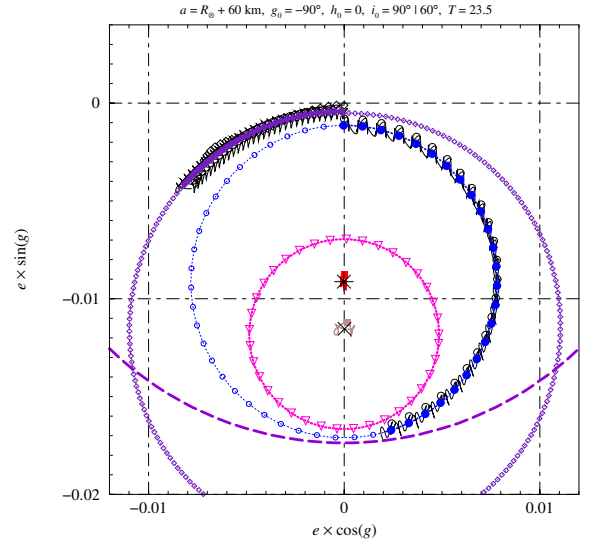


Figure 9: Orbital evolution (thin black lines) for $i_0 = 90^\circ$ (circles) and $i_0 = 60^\circ$ (diamonds), started at $e_0 = 0.0008$ and $e_0 = 0.00001$ respectively, and $a_0 = R_\oplus + 60$ km. Both initially quasi-circular orbits eventually reach e_c (violet, dashed circle) and crash on the Martian surface after 23.5 day $_\oplus$ and 63 day $_\oplus$ respectively, due to the slow rotation of the eccentricity vector (blue and indigo symbols) around the respective FOs (star and cross) and POs (red and brown curves). For the polar orbit, it is the small periodic component that actually causes the crash. The crash for $i_0 = 60^\circ$ is detected using an integration up to $T = 30$ day $_\oplus$, thanks to the fitting/extrapolation properties of Prony’s method. An orbit started at the location of the FO of the ‘ J_2 & J_3 problem’ (magenta curve) at $i_0 = 60^\circ$ only barely avoids crashing.

6. Dynamics near low-altitude POs

POs (and FOs) are interesting for practical purposes, as they dictate the dynamics in their phase-space neighborhood. For low altitudes in particular, the location of a PO can cause a quasi-circular orbit to crash on the primary’s surface. This unobvious effect was already noticed by Knežević and Milani (1998), who studied the crash of an Apollo 16 subsatellite on the Moon after 34 days, while the nominal mission duration for 100 km altitude was one year. The crash was caused by a continuous growth of the subsatellite’s eccentricity, that Knežević and Milani (1998) showed originating from $l > 3$ -degree gravity terms that result into a slow rotation of the eccentricity vector around the corresponding FO. Hence, as shown below, having accurate positions of FOs or POs, we can build ‘dynamical fate’ maps for all initial conditions in their neighborhood.

6.1. Dynamics around FOs/POs

Orbits started at (e_p, g_p) (or (e_F, g_F) for 20ZM) have zero proper amplitude α_s while, for any other initial condition (e_0, g_0) , they have³ $|\alpha_s| \approx |e_0 \sin(g_0) - e_p \sin(g_p)|$.

When g_0 and g_p have the same sign, the proper amplitude is $\alpha_s = |e_0 - e_p|$. For initial e_0 satisfying $e_c >$

³In this section, we restrict ourselves to cases with $g_0 = \pm 90^\circ$

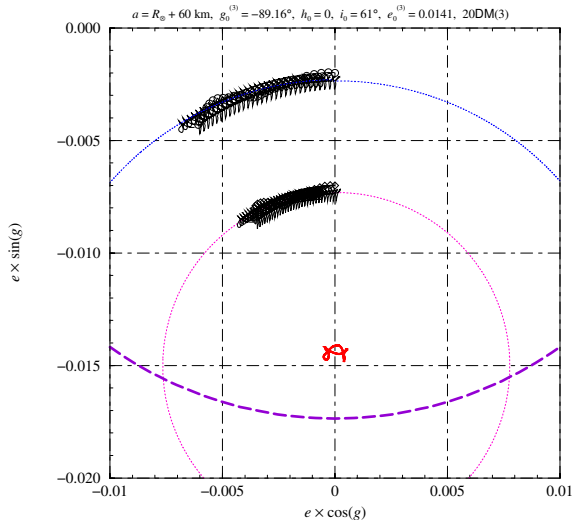


Figure 10: Orbital evolution (thin black lines and circles) for $i_0 = 61^\circ$ and $e_0 = 0.002$; the orbit collides with Mars after 79 day_\oplus (violet dashed circle denotes the collision line). Another orbit, started at $e_0 = 0.007$ (the FO of the ‘ J_2 & J_3 problem’) also crashes after 88 day_\oplus (dotted magenta curve). The PO obtained after 3 iterations of our filtering algorithm (red line) will never crash on the Martian surface, and stays around the ‘nearly-frozen’ parameters $g = -89^\circ$, $e = 0.0141$, having excursions in eccentricity $\approx \pm 0.0005$.

$e_0 > e_p$, we will then have $e(t)$ slowly oscillating within e_0 and $2e_p - e_0 < e_0$, with g circulating if $e_0 - e_p > e_p$ and librating otherwise. On the other hand, for $e_0 < e_p$, the slow rotation around the PO lifts the eccentricity up to $2e_p - e_0 > e_0$; the satellite will crash if this is larger than e_c . Thus, if the PO has $e_p > e_c/2$, orbits with $e_0 < 2e_p - e_c$ (e.g. a circular orbit) will crash on Mars surface in less than $T_s/2$; this is essentially what [Knežević and Milani \(1998\)](#) found, while studying the crash of the Apollo 16 subsatellite on the Moon. This is exemplified in figure 9, for two quasi-circular low-altitude orbits around Mars at inclinations $i_0 = 90^\circ$ and $i_0 = 60^\circ$, both of which crash in less than $T_s(i_0)/2$. Note that the slow period $T_s(i_0)/2$ depends strongly on i_0 , becoming very large at $i_c \approx 63.4^\circ$. Yet, this period will be only 25 Martian days at $i_0 = 90^\circ$ and at most 100 day_\oplus as soon as $|i_0 - i_c| > 3^\circ$. On the other hand, the PO itself will keep its eccentricity nearly constant and will never crash.

Another example is shown in figure 10 where a slowly evolving orbit close to the critical inclination i_c starting at low eccentricity nevertheless crashes after 79 day_\oplus (about 3 times the orbit arc used in Prony’s FA), as the PO is very close to the collision limit. Choosing a circular orbit or the FO of the ‘ J_2 & J_3 problem’ as initial condition, as is often done for preliminary design, the orbit would again crash, showing that these approximations should always be complemented by other methods including higher-degree terms of the gravitational potential at low altitudes, as also advocated in ([Lara et al., 2013](#)). The true PO found by our algorithm is indeed stable and safe from collision.

For orbits starting with opposite sign for g_0 with re-

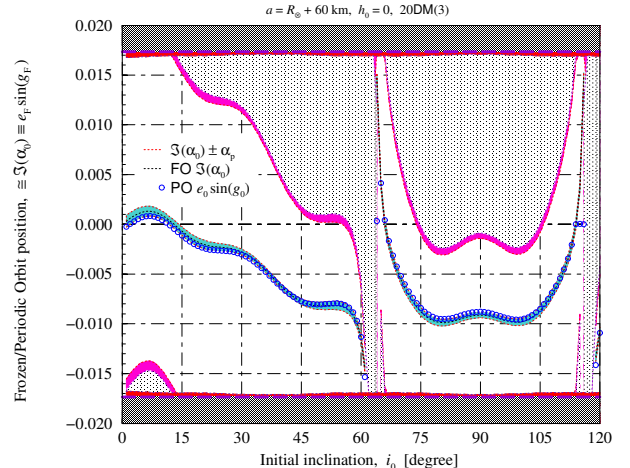


Figure 11: Dynamical fate map, showing the survivability of low-altitude Martian orbits, in the $i_0 - e_0 \sin g_0$ plane. Blue circles are the POs; the dashed line represents the orbits mean position $e_F \sin g_F$ (FOs). These orbits are long-lived, as eccentricity excursions are within the turquoise band ($\pm \alpha_p$). Orbits in the white zones are also long-lived, with eccentricity excursions of order $2\delta e_F$ around the PO. The magenta zones contain initial conditions that collide with Mars in less than $T_s/2 + T_{\text{rot}}$. In the dotted zones, orbits will collide in less than $T_s/2$ while, in the red zones, orbits would collide in less than T_{rot} . In the grey zones, orbits are already above e_c .

spect to g_p , the situation is worse, as $|\alpha_s| = |e_0 + e_p|$, i.e. e_0 is pushed up to $2e_p + e_0$ and the satellite crashes if this value is larger than e_c . Hence, orbits with $e_0 > e_c - 2e_p$ will crash on Mars and, for $e_p \geq e_c/2$, all orbits with that (wrong) sign of g_0 – even with $e_0 \approx 0$ – will also crash. Moreover, if e_p reaches e_c , any orbit will crash in less than $T_s/2$ whatever its initial eccentricity e_0 or the sign of its initial pericenter argument g_0 .

From the above analysis it is evident that the PO position conditions the existence of non-collisional orbits at low altitudes, as well as the extent to which active control needs to be used, in order to control eccentricity and altitude variations.

6.2. Dynamical fate maps

Using the results presented in the previous sections, we can build ‘*dynamical fate maps*’ that immediately display the survivability of orbits around POs. An example is given in figure 11, as a projection on the $(i_0, e_0 \sin g_0)$ plane, for $a = R_\oplus + 60 \text{ km}$.

Let us describe all orbital regions, shown on this map by different color/texture. We know that a PO at given i_0 is stable and does not lead to collision as, in general, the periodic terms have amplitudes of order $\alpha_p \approx 10^{-3}$ (the turquoise band in figure 11). To fix ideas, consider $g_p > 0$, as is the case in figure 11 for $0 < i_0 < 13^\circ$. If we move to ‘higher’ positions $e_c > e_0 > e_p$ (white zone above the PO), the orbit will oscillate between e_0 and $2e_p - e_0$ (with the latter negative for large e_0) but will never reach the (lower) collision eccentricity $-e_c$, so the orbit will live forever with eccentricity variations $|e_0 - e_p|$. If we now move to ‘lower’

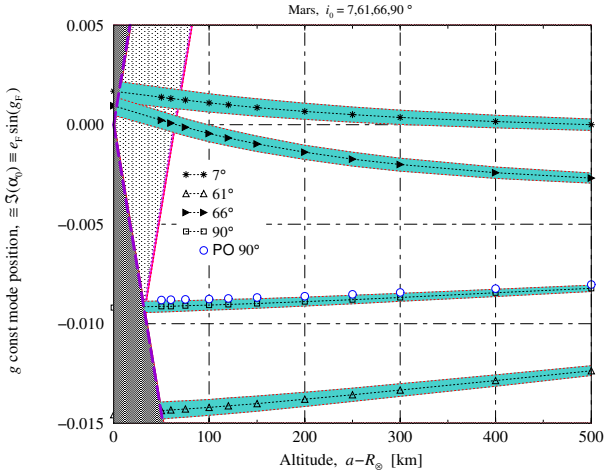


Figure 12: Displacement of FOs (i.e. mean positions of POs) locations as a function of the altitude $a_0 - R_{\oplus}$ for different initial inclinations $i_0 = 7^\circ$, $i_0 = 61^\circ$, $i_0 = 66^\circ$ and $i_0 = 90^\circ$. Orbits in the shaded grey zones exceed e_c (thick, dashed violet line). The POs (blue circles) and the dynamical fate zones are plotted for $i_0 = 90^\circ$ (the bands of width $\pm\alpha_p$ are invisible at this scale). The PO eccentricity reaches $e_p = e_c$ at about 33 km altitude for polar orbits.

positions $e_0 \sin g_0$, including those for which g_0 is negative (white zone below the PO), the orbits will still live forever, but will oscillate in e with an amplitude $|\alpha_s| \approx |e_0 \sin(g_0) - e_p|$. This amplitude increases when moving lower, until we reach position $-e_c + 2e_p + \alpha_p$, where the combined effect of proper and forced terms will cause the orbit to crash after at most $T_s/2 + T_{rot}$ (magenta zones in figure 11). This zone has a height in eccentricity α_p and, as soon as we reach $-e_c + 2e_p$, orbits will collide in less than $T_s/2$, simply due to the slow proper motion (dotted zones in figure 11). Below $e_0 = -e_c + \alpha_p$ or above $e_c - \alpha_p$, the small periodic terms are enough to cause the orbit to crash in at most one rotation of Mars T_{rot} .

The map provides a rather complete picture of the dynamical fate, for all initial conditions at a given altitude. It explains both collision zones observed for $e_0 < e_c$ in figure 5, i.e. for $0 < i_0 < 13^\circ$ and $75^\circ < i_0 < 105^\circ$. It also shows that, for $61^\circ < i_0 < 65^\circ$, non-collisional orbits do not exist, as these POs would have $e_p > e_c$.

It is interesting to see how the map changes with altitude. There is no technical difficulty in building this map for any altitude. Maps of the entire space of initial conditions a_0, i_0, e_0 can be obtained efficiently using our method, but it is difficult to visualize the results in 3-d. We thus display a 2-d projection of these results in the $(a_0, e_0 \sin g_0)$ space, for selected inclinations i_0 in figure 12. Note that the initial conditions for the POs are expected to be smooth functions of a_0 , as for i_0 . In fact, this implies that the whole 3-d map can be computed by continuation, starting only from a single guess, locating a PO at some altitude and i_0 , then using this as initial guess for an adjacent value of i_0 , etc. When the inclination range is exhausted, we can start incrementing the altitude, repeating the above procedure.

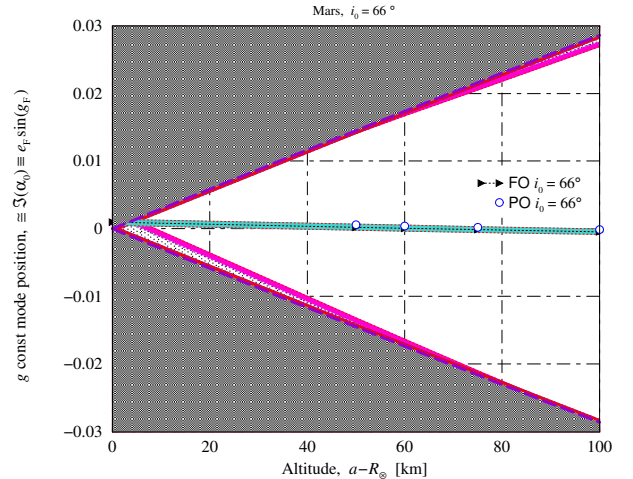


Figure 13: Dynamical fate map for $i_0 = 66^\circ$. The PO is located at nearly zero eccentricity. Symbols and zones color codes are the same as in figure 11. Orbits could survive down to 6 km altitude.

The displacement of FOs (i.e. mean positions of POs) and of the initial conditions of POs with altitude is non-trivial. While the size of the fast terms α_p is decreasing monotonically with altitude, the FOs displacement is more complicated; this is not so surprising as in the axisymmetric case the FO location can be found by numerically solving a strongly non-linear equation, whose coefficients depend on altitude (see e.g. Lara et al. (2009)). Still, this shift is small at low altitudes, while e_c is proportional to $a_0 - R_{\oplus}$. Thus, there is always an altitude for which $e_p \geq e_c$ and no orbit can survive below. A dynamical fate map for polar orbits is displayed in figure 12 as a function of altitude. As one can see, polar Martian orbits are safe down to $a_0 = R_{\oplus} + 33$ km, with $e \approx 0.008$. This orbit resembles the one of the Global Mars Surveyor (GMS), but at a much lower altitude. Note that, for polar orbits, e_p varies very little with altitude, so it remains roughly the same also at the GMS altitude (372 km).

Near-frozen, quasi-circular orbits at very low altitudes ($\lesssim 10$ km) are possible, but only for selected inclinations. As seen in figure 12, this is the case for $i_0 \approx 13^\circ$ and $i_0 \approx 66^\circ$. The dynamical fate map for $i_0 = 66^\circ$ is shown in figure 13. In principle, non-crashing orbits down to 6 km can be found, but the Martian topography would certainly not allow it.

7. Conclusions – Discussion

In this paper we presented a detailed study of low Martian orbiters ($a - R_{\oplus} < 500$ km), applying Prony's Frequency Analysis and an iterative filtering algorithm that allowed effective computation of families of periodic orbits that dominate the secular dynamics of nearly circular satellite orbits. Our main goal was to present an effective way of describing eccentricity variations and determining the dynamical fate of orbits, such that it could be useful for preliminary orbit design. As high-eccentricity orbits

cannot have near-constant altitude, our primary focus was on the 2-d.o.f. equivalent of frozen orbits, namely nearly-frozen periodic orbits.

By performing a series of tests, we found the 'minimal' model for the Martian gravity field to be of degree $l_{\max} = 20$ and studied both the full model (2ODM) and its axisymmetric counterpart (2OZM). In contrast to the Moon, we find that the Martian gravity field can be well approximated by an axisymmetric model, even for satellites at altitudes $\lesssim 60$ km, with the exception maybe of near-equatorial orbits ($i \leq 13^\circ$). Nevertheless, the true secular motion is described by two vectors (the complex $u(t)$ and $v(t)$ in our notation), although weakly coupled in most cases, and an accurate representation of both should be given.

In the absence of exact analytical solutions for the high-order and degree 2-d.o.f. problem, Prony's frequency analysis is a very effective method of accurately computing a quasi-periodic fit of the secular orbit. The separation of the two main frequencies guarantees that low-order linear combinations (resonances) will not 'contaminate' the signal and the motion will be regular. Prony's method has some advantages over other spectral methods, namely it requires only a very short orbit arc to produce an accurate determination of the fundamental modes (frequencies and amplitudes). Moreover, under the same assumption of frequency separation, it can be easily complemented by an iterative filtering method, which allows efficient determination (2–3 iterations) of periodic orbits, in the vicinity of any initial condition. Note that, apart from locating the POs, it also provides a very precise decomposition of these orbits, which contains only low-amplitude, 'fast', periodic variations around the mean position. The constructive theory of Wiesel (2012) explains the frequency decomposition of POs and provides ground for the convergence of our iterative algorithm. Unlike differential corrections, our method unfortunately does not provide direct indication of linear stability for the POs. On the other hand, the correction steps are independent of the complexity of the gravity model considered.

A collection of POs for different altitudes and inclinations, projected on the $(e \cos g, e \sin g)$ plane, is given in figure 14. Because PO positions are smooth functions of the initial conditions, one can compute a full 3-d map of POs (in a , e and i) by continuation, starting from a first guess and smoothly varying the parameters of the family of POs. While the overall computational burden is certainly higher than e.g. solving a nonlinear equation of high degree to find the FOs of an axisymmetric model, the gain in precision, but mostly in acquiring also the spectral decomposition of the true secular orbit, is considerable. Using the information on relative amplitudes, one can construct and fully describe 'dynamical fate maps' for satellite orbits at any given altitude and inclination. These maps can be seen as a generalization of the classical inclination–eccentricity diagrams and are a potentially useful tool for preliminary mission design.

Figure 12, for example, confirms that the Global Mars Surveyor orbit ($i = 93^\circ$, $e = 0.008$, minimum altitude 372 km) keeps very close to the corresponding PO and has eccentricity variations of only $\simeq 10^{-3}$ – smaller than at most other inclinations for the same altitude – and altitude variations of ≈ 60 km. The Exomars Trace Gas Orbiter ($i = 74^\circ$, $e = 0$, altitude 400 km) and Mars Odyssey ($i = 93^\circ$, $e = 0$, altitude 400 km) require active control to suppress altitude variations, as they are located at $\delta e_F \approx 0.008$ from the PO, and hence have eccentricity variations $2\delta e_F \approx 0.016$ and altitude variations of ≈ 120 km; still, the collision eccentricity is ≈ 0.1 at 400 km altitude and so these satellites are safe. However, figure 11 suggests that the same strategy (i.e. choosing $e = 0$) would become inefficient at lower altitudes and, in fact, for $i = 74^\circ$ or 93° and initial altitudes ≤ 70 km, a circular orbit would swiftly crash on Mars.

In conclusion, we believe that our method can be an effective tool for preliminary trajectory design. We plan to explore it further — considering other solar system objects as targets — and report in a forthcoming paper.

7.1. Acknowledgements

We are grateful to the anonymous reviewers for their thorough reviews that helped us improve our paper. Many thanks go to S. Tzirti for assisting us with numerical integrations used in this study, even long after having left the field.

References

- Abad, A., Elife, A., Tresaco, E.: Analytical model to find frozen orbits for a lunar orbiter. *JGCD* **32**(3), 888–898 (2009) [1](#)
- Allan, R. R.: The Critical Inclination problem: A simple treatment. *Celest. Mech.* **2**, 121–122 (1970) [1](#)
- Broucke, R.A.: Numerical integration of periodic orbits in the main problem of artificial satellite theory. *Celest. Mech. Dyn. Astron.* **58**, 99–123 (1994) [5](#)
- Coffey, S.L., Deprit, A., & Miller, B.R.: The critical inclination in artificial satellite theory. *Celest. Mech.* **39**, 365–406 (1986) [1](#), [5](#)
- Coffey, S.L., Deprit, A., & Deprit, E.: Frozen orbits for satellites close to an Earth-like planet. *Celest. Mech. Dyn. Astron.* **59**, 37–72 (1994) [1](#)
- Couetdic, J., Laskar, J., Correia, A.C.M., Mayor, M., & Udry, S.: Dynamical stability analysis of the HD202206 system and constraints to the planetary orbits. *A&A* **519**, A10 1–14 (2010) [1](#)
- Delsate, N., Robutel, P., Lemaître, A., & Carletti, T.: Frozen orbits at high eccentricity and inclination: application to Mercury orbiter. *Celest. Mech. Dyn. Astron.* **108**, 275–300 (2010) [1](#), [4](#)
- Delsate, N.: Analytical and numerical study of the ground-track resonances of Dawn orbiting Vesta. *Plan. and Space Science* **59**, 1372–1383 (2011) [1](#)
- Deprit, A., & Henrard, J.: Natural families of periodic orbits. *Astron. J.* **72**, 158–172 (1967) [1](#)
- De Saedeleer, B.: Complete Zonal problem of the artificial satellite: Generic compact analytic first order in closed form. *Celest. Mech. Dyn. Astron.* **91**, 239–268 (2005) [1](#), [2.2](#)
- De Saedeleer, B.: Analytical theory of a lunar artificial satellite with third body perturbations. *Celest. Mech. Dyn. Astron.* **95**, 407–423 (2006) [2.2](#)
- Dufey, J., Noyelles, B., Rambaux, N., & Lemaître, A.: Latitudinal librations of Mercury with a fluid core. *Icarus* **203**, 1–12 (2009) [1](#)

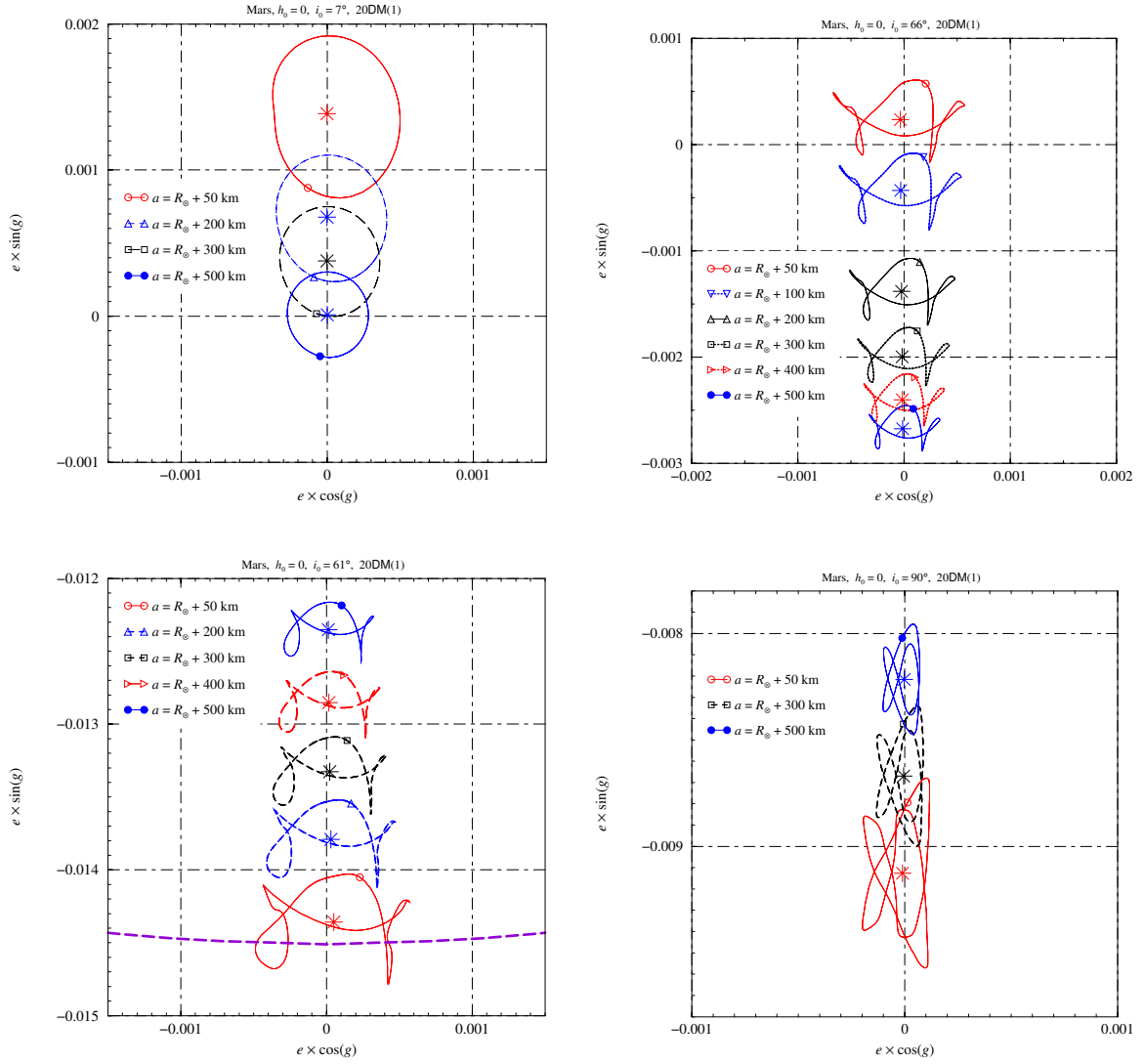


Figure 14: *Periodic Orbits* for different values of $a_0 - R_{\oplus} < 500$ km and i_0 : 7° (top left), 61° (bottom left), 66° (top right) and 90° (bottom right). With decreasing altitude, the PO's mean position (FO, crosses) can move to higher (for $i_0 = 7^\circ$, 61° or 90°) or lower eccentricities ($i_0 = 66^\circ$). At lower altitudes, the periodic terms increase in amplitude and the projection of the orbit becomes more and more involved; FA can accurately describe this behavior. For $i_0 = 61^\circ$ and 50 km altitude the satellite would crash on Mars.

- Elife, A., & Lara, M.: Frozen Orbits About the Moon. *J. Guid. Control Dyn.* **26**(2), 238–243 (2003) [2.2](#)
- Garfinkel, B.: Tesseral Harmonic Perturbations of an Artificial Satellite. *Astron. J.* **70**, 784–786 (1965) [1](#)
- Gurfil, P., & Lara, M.: Motion near frozen orbits as a means for mitigating satellite relative drift. *Celest. Mech. Dyn. Astron.* **116**, 213–227 (2013) [1, 5](#)
- Gurfil, P., & Seidelmann, P.K.: *Celestial Mechanics and Astrodynamics: Theory and Practice*. Springer-Verlag, Berlin (2016). [1, 1, 2.1, 5](#)
- Genova, A., Goosens, S., Lemoine, F.G., Mazarico, E., Neumann, G.A., Smith, D.E. & Zuber, M.T.: Seasonal and static gravity field of Mars from MGS, Mars Odyssey and MRO radio science. *Icarus* **272**, 228–245 (2016) [1, 2.2](#)
- Hamming, R.W.: *Numerical Methods for Scientists and Engineers*. Dover (1973). [3.1, 3.1](#)
- He, Y., Xu, M., Jia, X., & Armellin, R.: High-precision repeat-groundtrack orbit design and maintenance for Earth observation missions. *Celest. Mech. Dyn. Astron.* **128**, 275–294 (2017) [1](#)
- Hildebrand, F.B.: *Introduction to Numerical Analysis* (2nd ed.). Dover (1987). [3.1, 3.1](#)
- Hughes, S.: The ‘Critical Inclination’: Another Look. *Celest. Mech.* **25**, 235–266 (1981) [1](#)
- Jupp, A. H.: The Critical Inclination problem — 30 years of progress. *Celest. Mech.* **43**, 127–138 (1988) [1](#)
- Kaula, W. M.: *Theory of Satellite Geodesy*. Blaisdell, Boston (1966). [1, 2.2, 2.2, 1, 2.2](#)
- Kay, S.M.: *Modern Spectral Estimation: Theory and Application*. Prentice Hall (1988). [3.1, 3.1](#)
- Knežević, Z., & Milani, A.: Orbit maintenance of a lunar polar orbiter. *Planet. Space Sci.* **46**, 1605–1611 (1998) [1, 2.2, 4, 6, 6.1](#)
- Konopliv, A.S., Yoder, C.F. & Standish, E.M.: A global solution for the Mars static and seasonal gravity, Mars orientation, Phobos and Deimos masses, and Mars ephemeris. *Icarus* **182**, 23–50 (2006) [2.2](#)
- Konopliv, A.S., Asmar, S.W., Folkner, W.M., Karatekin, O., Nunes, D.C., Smrekar, S.E., Yoder, C.F. & Zuber, M.T.: Mars high resolution gravity fields from MRO, Mars seasonal gravity, and other dynamical parameters. *Icarus* **211**, 401–428 (2011) [2.2](#)
- Konopliv, A.S., Park, R.S. & Folkner, W.M.: An improved JPL Mars gravity field and orientation from Mars orbiter and lander tracking data. *Icarus* **274**, 253–260 (2016) [1, 2.2](#)
- Lara, M.: On Periodic Polar Orbits in the Artificial Satellite Problem. *J. of Astronaut. Sci.* **45**, 321–328 (1997) [1](#)
- Lara, M.: Searching for Repeating Ground Track Orbits: A Systematic Approach. *J. of Astronaut. Sci.* **47**, 177–188 (1999) [1](#)
- Lara, M.: Repeat Ground Track Orbits of the Earth Tesseral Problem as Bifurcations of the Equatorial Family of Periodic Orbits. *Celest. Mech. Dyn. Astron.* **86**, 143–162 (2003) [1](#)
- Lara, M.: Design of long-lifetime lunar orbits: A hybrid approach. *Acta Astronaut.* **69**, 186–199 (2011) [1, 2.2](#)
- Lara, M.: Exploring Sensitivity of Orbital Dynamics with Respect to Model Truncation: The Frozen Orbits Approach. *Astrophys. and Space Sci. Proc.* **52**, 69–83 (2018) [1, 2.2](#)
- Lara, M., & Peláez, J.: On the numerical continuation of periodic orbits - an intrinsic, 3-dimensional, differential, predictor-corrector algorithm. *Astron. Astroph.* **389**, 692–701 (2002) [1](#)
- Lara, M., & Russell, R.P.: Fast Design of Repeat Ground Track Orbits in High-Fidelity Geopotentials. *J. of Astronaut. Sci.* **56**, 311–324 (2008) [1](#)
- Lara, M., De Saedeleer, B., & Ferrer, S.: Preliminary design of low lunar orbits. In: *Proceedings of the 21st international symposium on space flight dynamics*, edited by the CNES, Sep.–Oct. 2009 (2009). [2.2, 5.2, 6.2](#)
- Lara, M., Ferrer, S. & De Saedeleer, B.: Lunar Analytical Theory for Polar Orbits in a 50-Degree Zonal Model Plus Third-Body Effect. *J. of Astronaut. Sci.* **57**, 561–577 (2009) [1](#)
- Lara, M., San-Juan, J.F., & López-Ochoa, L.M.: Precise Analytical Computation of Frozen-Eccentricity, Low Earth Orbits in a Tesseral Potential. *Math. Prob. Eng.* **2013**, 191384:1–13 (2013) [1, 4, 6.1](#)
- Lara, M., López, R., Pérez, I., & San-Juan, J.F.: Exploring the long-term dynamics of perturbed Keplerian motion in high degree potential fields. *Commun. Nonlinear Sci. Numer. Simulat.* **82**, 105053:1–18 (2020) [1, 2.2, 2.2](#)
- Laskar, J.: The chaotic behaviour of the solar system: A numerical estimate of the size of the chaotic zones. *Icarus* **88**, 266–291 (1990) [1, 3](#)
- Laskar, J.: Frequency Map Analysis and quasiperiodic decompositions. In: *Hamiltonian systems and Fourier analysis*, eds. D. Benest, C. Froeschlé, & E. Lega, Cambridge Scientific Publishers (2005) [3](#)
- Laskar, J., Froeschlé, C., & Celletti, A.: The measure of chaos by the numerical analysis of the fundamental frequencies. Application to the standard mapping. *Physica D* **56**, 253–269 (1992) [3](#)
- Lemoine, F.G., Smith, D.E., Rowlands, D.D., Zuber, M.T., Neumann, G.A., Chinn, D.S. & Pavlis, D.E.: An improved solution of the gravity field of Mars (GMM-2B) from Mars Global Surveyor. *J. Geophys. Res.* **106**(E10), 23359–23376 (2001) [2.2](#)
- Liu, X., Baoyin, H. & Ma, X.: Five Special Types of Orbits Around Mars. *J. Guid. Control Dyn.* **33**(4), 1294–1301 (2010) [1](#)
- Liu, X., Baoyin, H. & Ma, X.: Analytical investigations of quasi-circular frozen orbits in the Martian gravity field. *Celest. Mech. Dyn. Astron.* **109**, 303–320 (2011) [1, 2.2](#)
- Liu, X., Baoyin, H. & Ma, X.: Periodic orbits around areostationary points in the Martian gravity field. *Research in Astron. Astrophys.* **12**(5), 551–562 (2012) [1](#)
- Murray, C.D., & Dermott, S.F.: *Solar System Dynamics*. Cambridge University Press, Cambridge (1999). [1](#)
- Noullez, A.: Chaos Characterization in Hamiltonian Systems using Resonance Analysis. In: *Dynamics of Celestial Bodies*, eds. H. Varvoglis, & Z. Knežević, Thessaloniki (2009) [3.1](#)
- Noullez, A., Tsiganis, K., & Tzirti, S.: Satellite orbits design using frequency analysis. *Advances in Space Research* **56**, 163–175 (2015) [1, 2, 2.2, 3.1, 5, 5.1, 5.1](#)
- Noyelles, B.: Expression of Cassini’s third law for Callisto, and theory of its rotation. *Icarus* **202**, 225–239 (2009) [1](#)
- Noyelles, B., Delsate, N., & Carletti, T.: Equilibrium search algorithm of a perturbed quasi-integrable system. <http://arxiv.org/pdf/1101.2138.pdf>, submitted to *Physica D* (2012) [5.1](#)
- de Prony, G.R.: Essai expérimental et analytique: sur les lois de la dilatabilité de fluides élastiques et sur les celles de la force expansive de la vapeur de l’eau et de la vapeur de l’alkool, à différentes températures. *J. Ec. Polytech.* **1-2** An. III, 24–76 (1795) [3.1](#)
- Robutel, P., Rambaux, N., & Castillo-Rogez, J.: Analytical description of physical librations of saturnian coorbital satellites Janus and Epimetheus. *Icarus* **211**, 758–769 (2011) [1](#)
- Russell, R.P., & Lara, M.: Long-Lifetime Lunar Repeat Ground Track Orbits. *J. Guid. Control Dyn.* **30**(4), 982–993 (2007) [1](#)
- San-Juan, J.F., Abad, A., Elife, A., Tresaco, E.: Analytical Model for Lunar Orbiter. *Adv. Astron. Sci.* **130**, 1281–1299 (2008) [1](#)
- San-Juan, J.F., Gavín, Á., López, L.M., & López, R.: *PPKBZ9^{A,S4}* Two Orbit Propagators Based on an Analytical Theory. *J. of Astronaut. Sci.* **58**, 643–660 (2011) [1](#)
- Tzirti, S., Tsiganis, K., & Varvoglis, H.: Quasi-critical orbits for artificial lunar satellites. *Celest. Mech. Dyn. Astron.* **104**, 227–239 (2009) [2](#)
- Tzirti, S., Tsiganis, K., & Varvoglis, H.: Effect of 3rd-degree gravity harmonics and Earth perturbations on lunar artificial satellite orbits. *Celest. Mech. Dyn. Astron.* **108**, 389–404 (2010) [1, 2, 2.2](#)
- Tzirti, S., Noullez, A., & Tsiganis, K.: Secular dynamics of a lunar orbiter: a global exploration using Prony’s frequency analysis. *Celest. Mech. Dyn. Astron.* **118**, 379–397 (2014) [1, 2, 2.2, 3, 3.1, 3.1, 3.2](#)
- Wiesel, W.E.: A Theory of Low Eccentricity Earth Satellite Motion. *J. of Astronaut. Sci.* **59**, 629–649 (2012) [1, 7](#)
- Zhou, C., Yu, S. & Liu, L.: Analytical Solution of Coupled Perturbation of Tesseral Harmonic Terms of Mars’s Non-spherical Gravitational Potential. *Chinese Astron. and Astrophys.* **36**, 399–407 (2012) [1](#)